UCLA
UCLA Previously Published Works

Title

MPR-Diff: A Self-Supervised Diffusion Model for Multi-Planar Reformation in Prostate Micro-Ultrasound Imaging

Permalink

https://escholarship.org/uc/item/0sx7f9xm

Journal

2011 IEEE International Symposium on Biomedical Imaging: From Nano to Macro, 00

ISSN

1945-7928

Authors

Pang, Kaifeng
Miao, Qi
Hung, Alex Ling Yu
et al.

Publication Date

2025-04-01

DOI

10.1109/isbi60581.2025.10981012

Peer reviewed

eScholarship.org Powered by the California Digital Library
University of California

Author Manuscript

Author Manuscript

Author Manuscript

Author Manuscript

HHS Public Access

Author manuscript

Proc IEEE Int Symp Biomed Imaging. Author manuscript; available in PMC 2025 May 26.

Published in final edited form as:

Proc IEEE Int Symp Biomed Imaging. 2025 April ; 2025: . doi:10.1109/isbi60581.2025.10981012.

MPR-DIFF: A SELF-SUPERVISED DIFFUSION MODEL FOR MULTI-PLANAR REFORMATION IN PROSTATE MICRO-ULTRASOUND IMAGING

Kaifeng Pang[⋆], **Qi Miao**[⋆], **Alex Ling Yu Hung**[⋆], **Kai Zhao**[⋆], **Eunsun Oh**[⋆], **Raymi Ramirez**[⋆], **Wayne Brisbane**[†], **Kyunghyun Sung**[⋆]

[⋆]Department of Radiological Sciences, UCLA, Los Angeles, CA, USA 90095

[†]Department of Urology, UCLA, Los Angeles, CA, USA 90095

Abstract

Micro-ultrasound (MicroUS) is a novel imaging technology with the potential to provide a low-cost and high-resolution approach for prostate cancer diagnosis. However, MicroUS is acquired in a non-uniform, fan-shaped sweep, where voxel size varies with distance from the probe and across slice angles. This irregular voxel distribution complicates reformatting into other imaging planes, making it challenging to conduct joint evaluations with other modalities such as MRI and histopathology. Existing interpolation-based reformatting methods lead to poor image resolution and introduce severe artifacts. In this paper, we propose **MPR-Diff**, a self-supervised diffusion model for super-resolution-based multi-planar reformation in prostate MicroUS imaging. Our method addresses the lack of high-resolution reference in the target plane by extracting simulated training patches from acquired slices. We performed both a quantitative evaluation and an expert reader study, demonstrating that our approach significantly enhances image resolution and reduces artifacts, thereby increasing the potential diagnostic value of MicroUS. Code is available at https://github.com/Calvin-Pang/MPR-Diff.

Index Terms—

Micro-ultrasound; Diffusion model; Super-resolution; Multi-planar reformation; Prostate

1. INTRODUCTION

Prostate cancer is the most frequently diagnosed cancer and the second-leading cause of cancer-related death among men in the United States [1, 2]. Conventional early diagnosis of prostate cancer relies on transrectal ultrasound (TRUS)-guided systematic biopsy, which has a short scan time but is limited to its low resolution and poor sensitivity to tumor detection [3]. Combining multi-parametric magnetic resonance imaging (mpMRI) with TRUS enables the accurate MRI-targeted biopsy and improves cancer diagnosis [3]. However, mpMRI is resource-intensive and requires a long scan time. Moreover, the low resolution of TRUS images makes accurate fusion with mpMRI challenging, often introducing registration errors that can hinder diagnosis [4].

Author Manuscript Author Manuscript Author Manuscript Author Manuscript

Micro-ultrasound (MicroUS) is an emerging 29-MHz ultrasound technology that is low-cost and offers 3–4 times higher resolution than traditional ultrasound imaging [3]. Recent studies [3, 5] suggest its potential to achieve a lower-cost diagnosis with comparable accuracy to mpMRI. Unlike the regularly spaced multi-slice volume of MRI, MicroUS acquires images in a fan-shaped manner, with slices obtained at non-uniform angular intervals (Figure 1). This acquisition approach is effective for cancer diagnosis but requires reformatting into other imaging planes for accurate comparison with modalities such as mpMRI, PET CT, and histopathology. The current method of multi-planar reformation (MPR) for MicroUS primarily relies on interpolation techniques, e.g., bilinear interpolation [3]. However, as shown in Figure 2, this approach faces two significant limitations: 1) the anterior region of the prostate, away from the probe, exhibits noticeable blurring due to attenuation of the ultrasound beam; and 2) the discontinuity between adjacent slices also degrade the image quality.

Deep learning (DL)-based image super-resolution (SR) is a promising technique to enhance low-resolution (LR) images into high-resolution (HR) images. Numerous SR models have been proposed for both natural images [6, 7] and medical images [8–10]. Among them, diffusion model-based methods [7–9] have shown impressive results due to their strong ability to generate realistic images with fine-grained details. However, little research has focused on using DL-based SR for MicroUS MPR, primarily due to the lack of HR target-plane images, which makes supervised model training challenging.

In this paper, we propose **MPR-Diff**, a diffusion model designed for multi-planar reformation in prostate MicroUS imaging. We also introduce a fully self-supervised training strategy that does not require HR target-plane images. Instead, we extract simulated LR and HR patches from the acquired slices to train the model. The main contributions of our research are as follows:

1. To the best of our knowledge, this is the first deep learning-based model for MicroUS multi-planar reformation.
2. Our method does not require HR target-plane images for supervision; instead, we train the model using simulated patches from slices in the original plane.
3. We conduct comprehensive experiments to evaluate the performance of our method. Both the quantitative results and qualitative reader study demonstrate that our approach effectively enhances resolution in the anterior region while reducing artifacts.

2. METHOD

2.1. Overview

We utilize a conditional Denoising Diffusion Probabilistic Model (DDPM) [7, 8, 11] to generate HR images conditioned on the LR counterparts. Considering the non-uniform and fan-shaped acquisition in MicroUS imaging, the spatial relationships between pixels can vary across the image. To address this, we incorporate the coordinates of the LR image pixels as a positional condition for the model. For the challenge of the lack of high-quality

Author Manuscript Author Manuscript Author Manuscript Author Manuscript

target-plane images, we propose a fully self-supervised patch-sampling training strategy. This approach randomly extracts LR-HR training pairs from real-acquired slices to simulate target-plane images.

2.2. Problem Statement

As illustrated in Figure 1, the MicroUS probe captures N slices, $\{s_1, s_2, \ldots, s_N\}$, each with a size of $H \times W$. Subsequently, after reformatting the acquired slices to represent the target plane, we obtain W LR fan-shaped images $M_{lr} \in \mathbb{R}^{H \times N}$. Here, we define **fan-shaped image** as a pixel matrix produced from a fan-shaped acquisition, where pixels are arranged based on angular coordinates θ and radial coordinates r, rather than a uniform Cartesian grid. $\theta \in [-\pi/2, \pi/2]$ denotes the angular position of pixels, while $r \in [0,1]$ represents the normalized radial distance from the probe.

In traditional MPR, M_{lr} is directly mapped to a Cartesian grid image I_{lr} through the interpolation. In our approach, we first use a diffusion model to upscale M_{lr} along the angular dimension to obtain an HR fan-shaped image $M_{hr} \in \mathbb{R}^{H \times kN}$, where k is the up-scaling factor. M_{hr} is then mapped to the Cartesian grid image I_{hr} using interpolation.

2.3. Conditional DDPM

Following previous works [7, 8, 11], we utilize the formulation of the conditional DDPM. The objective is to generate a target HR image $\boldsymbol{x}_0$ conditioned on a given LR image $\boldsymbol{y}$, where, in our case, $\boldsymbol{x}_0$ and $\boldsymbol{y}$ represent M_{hr} and M_{lr}, respectively. The conditional DDPM consists of two processes: a forward diffusion process q and a reverse denoising process p_θ parameterized by a neural network θ.

The forward process q is a Markovian noising process that iteratively adds noise to the target image $\boldsymbol{x}_0$ based on a variance schedule β_t:

$$q(\boldsymbol{x}_t \mid \boldsymbol{x}_{t-1}) = \mathcal{N}\left(\boldsymbol{x}_t; \sqrt{1-\beta_t}\boldsymbol{x}_{t-1}, \beta_t \boldsymbol{I}\right) \tag{1}$$

With Equation (1), we can directly sample x_t at an arbitrary timestep t:

$$q(\boldsymbol{x}_t \mid \boldsymbol{x}_0) = \mathcal{N}\left(\boldsymbol{x}_t; \sqrt{\bar{\alpha}_t}\boldsymbol{x}_0, (1-\bar{\alpha}_t)\boldsymbol{I}\right) \tag{2}$$

$$\boldsymbol{x}_t = \sqrt{\bar{\alpha}_t}\boldsymbol{x}_0 + \sqrt{1-\bar{\alpha}_t}\boldsymbol{\epsilon} \tag{3}$$

where $\alpha_t = 1 - \beta_t, \bar{\alpha}_t = \prod_{s=1}^{t} \alpha_s$, and $\boldsymbol{\epsilon} \sim \mathcal{N}(0, I)$.

Author Manuscript Author Manuscript Author Manuscript Author Manuscript

In the reverse denoising process p_θ, the goal is to infer $\boldsymbol{x}_{t-1}$ given $\boldsymbol{x}_t$ and the conditional image $\boldsymbol{y}$. Due to the non-uniform, fan-shaped acquisition of MicroUS, we utilize the coordinates of the LR image pixels, c, as an additional positional condition for the model. The reverse process can be parameterized as:

$$p_\theta(\boldsymbol{x}_{t-1} \mid \boldsymbol{x}_t, \boldsymbol{y}, c) = \mathcal{N}(\boldsymbol{x}_{t-1}; \boldsymbol{\mu}_\theta(\boldsymbol{x}_t, \boldsymbol{y}, c, t), \boldsymbol{\Sigma}_\theta(\boldsymbol{x}_t, \boldsymbol{y}, c, t)) \tag{4}$$

Following the formulation of [7], the super-resolution refinement is achieved by iteratively using the following form:

$$\boldsymbol{x}_{t-1} = \frac{1}{\sqrt{\alpha_t}}\left(\boldsymbol{x}_t - \frac{1-\alpha_t}{\sqrt{1-\bar{\alpha}_t}} f_\theta(\boldsymbol{x}_t, \boldsymbol{y}, c, t)\right) + \sqrt{1-\alpha_t}\boldsymbol{z} \tag{5}$$

where $\boldsymbol{z} \sim \mathcal{N}(0, I)$, and f_θ denotes the neural network.

2.4. Training and Inference

Due to the lack of HR target-plane reference, we propose a self-supervised patch-sampling training strategy, where we use randomly selected LR and HR polar coordinates to extract LR and HR training patches from acquired slices (Figure 4). The LR and HR patches are denoted as $\widetilde{\boldsymbol{M}}_{lr} \in \mathbb{R}^{h \times n}$ and $\widetilde{\boldsymbol{M}}_{hr} \in \mathbb{R}^{h \times kn}$, respectively.

In detail, to simulate the non-uniform angular coordinates of the target-plane fan-shaped image, we first randomly sample N angles between $-\pi/2$ and $\pi/2$ in ascending order: $\{\theta_1, \theta_2, \ldots, \theta_N\}$. From these, n consecutive angles are randomly selected as the LR angular coordinates $\left\{\tilde{\theta}^{lr}\right\}$, and the HR angles $\left\{\tilde{\theta}^{hr}\right\}$ are calculated as kn uniformly distributed angles within the range of $\left\{\tilde{\theta}^{lr}\right\}$:

$$\left\{\tilde{\theta}^{lr}\right\} = \{\theta_v, \theta_{v+1}, \ldots, \theta_{v+n-1}\} \tag{6}$$

$$\left\{\tilde{\theta}^{hr}\right\} = \{\theta_v, \theta_v + \Delta\theta, \theta_v + 2\Delta\theta, \ldots, \theta_{v+n-1}\} \tag{7}$$

where v is the starting index of $\left\{\tilde{\theta}^{lr}\right\}$, and $\Delta\theta = \frac{\theta_{v+n-1} - \theta_v}{kn-1}$.

Similar to angles, we randomly select h consecutive radial coordinates from the normalized radial coordinates $\{r_1, r_2, \ldots, r_H\}$:

Author Manuscript Author Manuscript Author Manuscript Author Manuscript

$$\{\tilde{r}\} = \{r_w, r_{w+1}, \ldots, r_{w+h-1}\} \tag{8}$$

As presented in Figure 4, using $\left\{\tilde{\theta}^{lr}\right\}$, $\left\{\tilde{\theta}^{hr}\right\}$, and $\{\tilde{r}\}$, we randomly extract LR and HR patches, $\widetilde{M}_{lr}$ and $\widetilde{M}_{hr}$, from the acquired slice, corresponding to $\boldsymbol{y}$ and $\boldsymbol{x}_0$ for training the model in Section 2.3.

During inference, we utilize the real LR fan-shaped image $M_{lr} \in \mathbb{R}^{H \times N}$ as the input to the model, along with angular coordinates $\{\theta\}$ and radial coordinates $\{r\}$. The model's output is the HR fan-shaped image $M_{hr} \in \mathbb{R}^{H \times kN}$.

3. EXPERIMENTS

3.1. Dataset and Setup

A total of 26 MicroUS studies were utilized in the experiments, each consisting of 150 to 300 slices with an in-plane resolution of 33.6 μm. 7 studies (1,716 slices in total) were used for training, and the MPR inference was conducted on the remaining 19 studies. All slices were originally acquired in the pseudosagittal plane, with the target reformation plane being the axial plane. All data were collected from clinical MircoUS scans at a single academic institution using an ExactVu MicroUS system (Exact Imaging, Markham, Ontario).

We implemented MPR-Diff using the U-Net [13] network from previous works [7, 8]. The model was trained and tested on a single NVIDIA Quadro RTX8000 GPU. We trained the model for 20 epochs using the Adam optimizer, with a learning of 5×10^{-6} and a batch size of 2. The up-scaling factor was set to $k = 8$, and the number of diffusion steps was set to 2×10^3. In each epoch, 10 pairs of LR and HR patches were randomly extracted from each slice for training. The spatial dimensions of $\widetilde{M}_{lr}$ and $\widetilde{M}_{hr}$ are set as 256 × 32 and 256 × 256, respectively.

3.2. Quantitative Results

We evaluated the quantitative performance with two metrics: sharpness and Perception-based Image Quality Evaluator (PIQUE) [15]. Sharpness was quantified using the Tenengrad measure [14], which calculates the average gradient magnitude by applying the Sobel filter in both horizontal and vertical directions. PIQUE [15] is a no-reference metric designed to access the perceptual image quality.

We included two state-of-the-art DL-based SR models, SwinIR [6] and SRConvNet [12], both of which were implemented using the same self-supervised training strategy and training protocol as MPR-Diff. As shown in Table 1, MPR-Diff significantly outperformed other competitors across both metrics, demonstrating that our method produces images with high sharpness and superior perceptual quality.

Author Manuscript Author Manuscript Author Manuscript Author Manuscript

3.3. Qualitative Analysis and Reader Study

Figure 5 presents the qualitative comparisons of a testing case that has a lesion in the anterior region. For reference, we also provide the corresponding annotated histopathology image. The lesion is highlighted in the red box of the MicroUS images. MPR-Diff significantly enhances the detail and boundary of the lesion. In contrast, other methods fail to improve the lesion's visualization, resulting in blurred anatomical details and unclear boundary. As indicated in the yellow box, MPR-Diff also reduces the slice discontinuity, whereas other methods show obvious inconsistency between adjacent slices.

To assess how MPR-Diff can enhance clinical diagnostic value, we conducted an expert reader study. For each testing study, reformatted images were generated using the bilinear interpolation and MPR-Diff, resulting in 38 evaluation cases (19 studies × 2 methods). With a few training sessions, one senior clinical urologist (W.B.) and one experienced radiologist specializing in urogenital imaging (M.Q.) independently assessed the image quality. All identifiers of patients and applied methods were removed and shuffled. The diagnostic image quality was assessed based on the four metrics: sharpness, noise, artifacts, and overall quality, each scored on a 5-point Likert scale (1: Nondiagnostic, 2: Poor, 3: Moderate, 4: Good, 5: Excellent). The readers evaluated the metrics from three perspectives: anterior, posterior, and whole gland.

Figure 6 presents the results of the expert reader study. The ratings were averaged between the two readers. The inter-reader variability, measured by Cohen's kappa coefficient [16], was 0.795, indicating substantial agreement between the two readers. MPR-Diff significantly enhanced the image quality in terms of sharpness, artifact reduction and overall quality in all prostate regions (especially in the anterior region), albeit with a slight increase in noise. Both qualitative analysis and reader study demonstrate our approach's potential for a higher diagnostic value compared to previous methods.

3.4. Ablation Study

We investigated the impact of key components in MPR-Diff by implementing the model with the following changes: (a) removing the positional condition (PC) from the diffusion model, and (b) replacing the random sampling of $\left\{\tilde{\theta}^{lr}\right\}$ with uniform sampling. As shown in Figure 7, without the positional condition, the model struggled to learn position-related information, resulting in severe artifacts. Moreover, when uniform sampling replaced the random sampling of $\left\{\tilde{\theta}^{lr}\right\}$, the model failed to learn the actual angular distribution of slices and produce images lacking fine-grained details.

4. CONCLUSION

In this paper, we proposed a self-supervised diffusion model, **MPR-Diff**, for multi-planar reformation in prostate Micro-ultrasound imaging. Our method eliminates the need for high-resolution target-plane images and significantly improves image quality compared to previous methods by using a patch-sampling training strategy. This approach can enhance the clinical value of MicroUS for prostate cancer diagnosis.

Author Manuscript Author Manuscript Author Manuscript Author Manuscript

5. COMPLIANCE WITH ETHICAL STANDARDS

Our experimental study was performed in compliance with the United States Health Insurance Portability and Accountability Act (HIPAA) of 1996 and was approved by the institutional review board (IRB) with a waiver of the requirement for informed consent.

ACKNOWLEDGMENTS

This research was funded in part by the National Institutes of Health under grants R01-CA248506 and R01-CA272702, and by the Integrated Diagnostics Program of the Departments of Radiological Sciences and Pathology in the UCLA David Geffen School of Medicine.

REFERENCES

[1]. Hung Alex Ling Yu, Zheng Haoxin, Miao Qi, Raman Steven S, Terzopoulos Demetri, and Sung Kyunghyun, “Cat-net: A cross-slice attention transformer model for prostate zonal segmentation in mri,” IEEE transactions on medical imaging, vol. 42, no. 1, pp. 291–303, 2022. [PubMed: 36194719]

[2]. Siegel Rebecca L, Giaquinto Angela N, and Jemal Ahmedin, “Cancer statistics, 2024.,” CA: a cancer journal for clinicians, vol. 74, no. 1, 2024.

[3]. Pensa Jake, Brisbane Wayne, Kinnaird Adam, Kuppermann David, Hughes Griffith, Ushko Derrick, Priester Alan, Gonzalez Samantha, Reiter Robert, Chin Arnold, et al. , “Evaluation of prostate cancer detection using micro-ultrasound versus mri through co-registration to whole-mount pathology,” Scientific Reports, vol. 14, no. 1, pp. 18910, 2024. [PubMed: 39143293]

[4]. Williams Cheyenne, Ahdoot Michael, Michael A Daneshvar Christian Hague, Wilbur Andrew R, Gomella Patrick T, Shih Joanna, Khondakar Nabila, Yerram Nitin, Mehralivand Sherif, et al. , “Why does magnetic resonance imaging-targeted biopsy miss clinically significant cancer?,” The Journal of urology, vol. 207, no. 1, pp. 95–107, 2022. [PubMed: 34433302]

[5]. Jiang Hongxu, Imran Muhammad, Muralidharan Preethika, Patel Anjali, Pensa Jake, Liang Muxuan, Benidir Tarik, Grajo Joseph R, Joseph Jason P, Terry Russell, et al. , “Microsegnet: A deep learning approach for prostate segmentation on micro-ultrasound images,” Computerized Medical Imaging and Graphics, vol. 112, pp. 102326, 2024. [PubMed: 38211358]

[6]. Liang Jingyun, Cao Jiezhang, Sun Guolei, Zhang Kai, Gool Luc Van, and Timofte Radu, “Swinir: Image restoration using swin transformer,” in Proceedings of the IEEE/CVF international conference on computer vision, 2021, pp. 1833–1844.

[7]. Saharia Chitwan, Ho Jonathan, Chan William, Salimans Tim, Fleet David J, and Norouzi Mohammad, “Image super-resolution via iterative refinement,” IEEE Transactions on Pattern Analysis and Machine Intelligence, vol. 45, no. 4, pp. 4713–4726, 2022.

[8]. Hung Alex Ling Yu, Zhao Kai, Zheng Haoxin, Yan Ran, Raman Steven S, Terzopoulos Demetri, and Sung Kyunghyun, “Med-cdiff: Conditional medical image generation with diffusion models,” Bioengineering, vol. 10, no. 11, pp. 1258, 2023. [PubMed: 38002382]

[9]. Zhao Kai, Pang Kaifeng, Hung Alex Ling Yu, Zheng Haoxin, Yan Ran, and Sung Kyunghyun, “Mri super-resolution with partial diffusion models,” IEEE Transactions on Medical Imaging, pp. 1–1, 2024.

[10]. Pang Kaifeng, Zhao Kai, Hung Alex Ling Yu, Zheng Haoxin, Yan Ran, and Sung Kyunghyun, “Nexpr: Neural explicit representation for fast arbitrary-scale medical image super-resolution,” Computers in biology and medicine, vol. 184, pp. 109354, 2025. [PubMed: 39602975]

[11]. Ho Jonathan, Jain Ajay, and Abbeel Pieter, “Denoising diffusion probabilistic models,” Advances in neural information processing systems, vol. 33, pp. 6840–6851, 2020.

[12]. Li Feng, Cong Runmin, Wu Jingjing, Bai Huihui, Wang Meng, and Zhao Yao, “Srconvnet: A transformer-style convnet for lightweight image super-resolution,” International Journal of Computer Vision, pp. 1–17, 2024.

[13]. Ronneberger Olaf, Fischer Philipp, and Brox Thomas, “U-net: Convolutional networks for biomedical image segmentation,” in Medical image computing and computer-assisted

Author Manuscript Author Manuscript Author Manuscript Author Manuscript

intervention–MICCAI 2015: 18th international conference, Munich, Germany, October 5–9, 2015, proceedings, part III 18. Springer, 2015, pp. 234–241.

[14]. Krotkov Eric, “Focusing,” International Journal of Computer Vision, vol. 1, no. 3, pp. 223–237, 1988.

[15]. Venkatanath Narasimhan, Praneeth D, Chandrasekhar Bh Maruthi, Channappayya Sumohana S, and Medasani Swarup S, “Blind image quality evaluation using perception based features,” in 2015 twenty first national conference on communications (NCC). IEEE, 2015, pp. 1–6.

[16]. Cohen Jacob, “A coefficient of agreement for nominal scales,” Educational and psychological measurement, vol. 20, no. 1, pp. 37–46, 1960.

Author Manuscript Author Manuscript Author Manuscript Author Manuscript

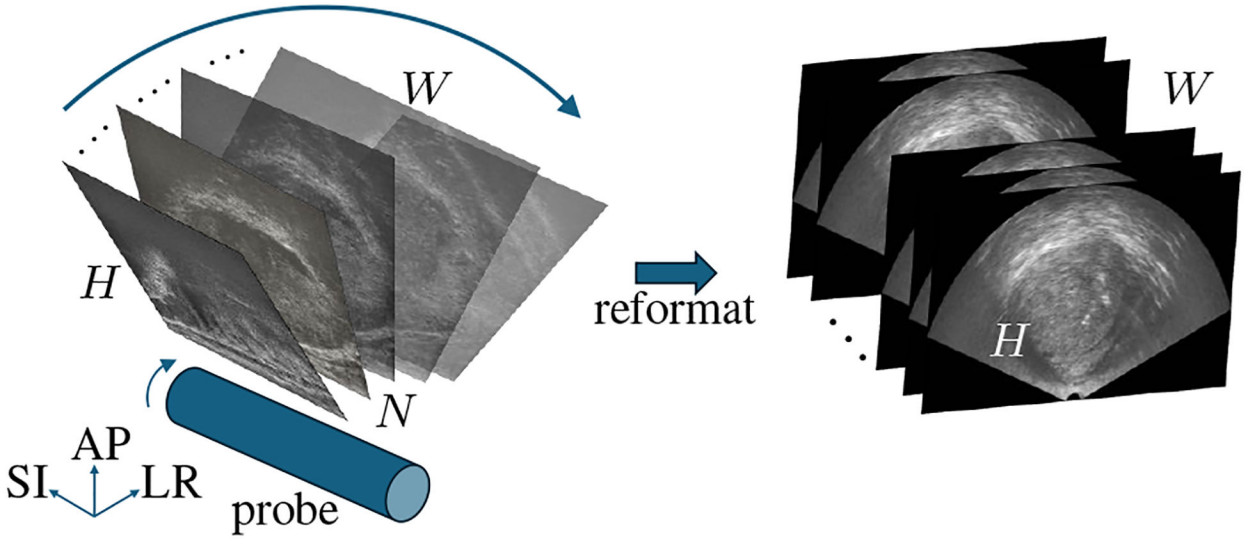

Fig. 1:
Example of MicroUS acquisition and multi-planar reformation. MicroUS uses the probe to capture slices spaced at non-uniform angular intervals in a fan-shaped sweep.

Author Manuscript Author Manuscript Author Manuscript Author Manuscript

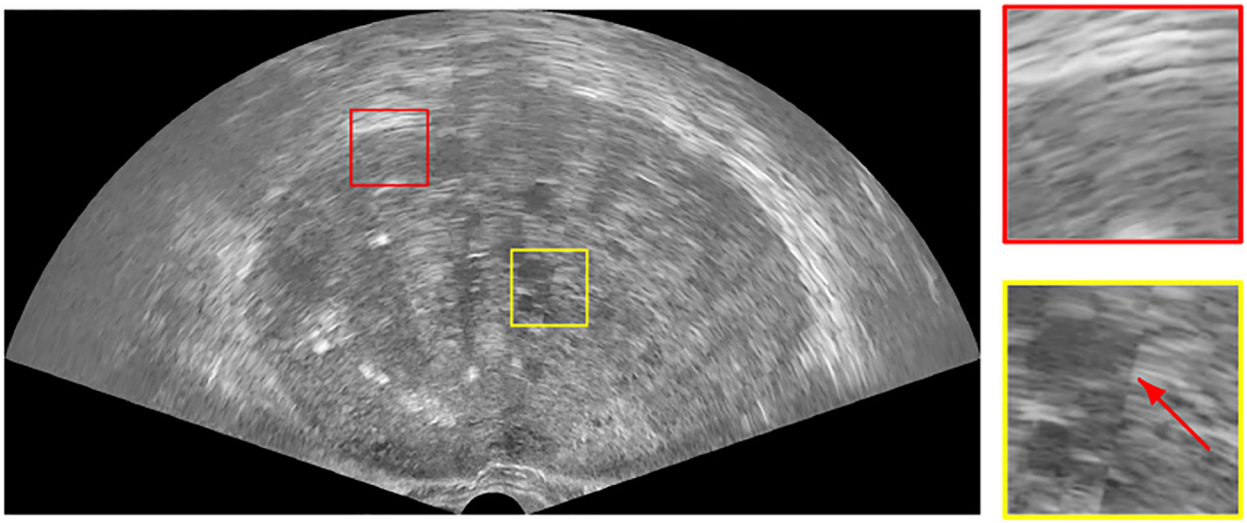

Fig. 2:
Interpolation reformation introduces blurring artifacts (red box) and slice discontinuity artifacts (yellow box).

Author Manuscript Author Manuscript Author Manuscript Author Manuscript

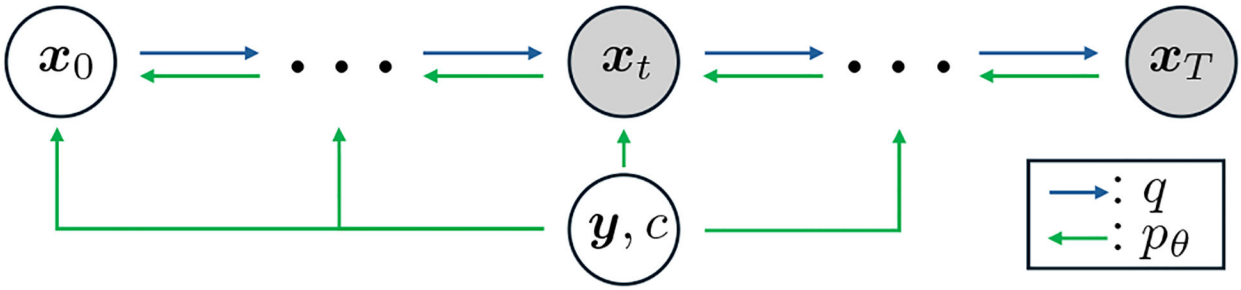

Fig. 3:

The graphical representation of the conditional diffusion model. The blue arrows represent the forward diffusion process q, while the green arrows indicate the inverse denoising process p_θ conditioned on the LR image $\boldsymbol{y}$ and LR coordinates c.

Author Manuscript Author Manuscript Author Manuscript Author Manuscript

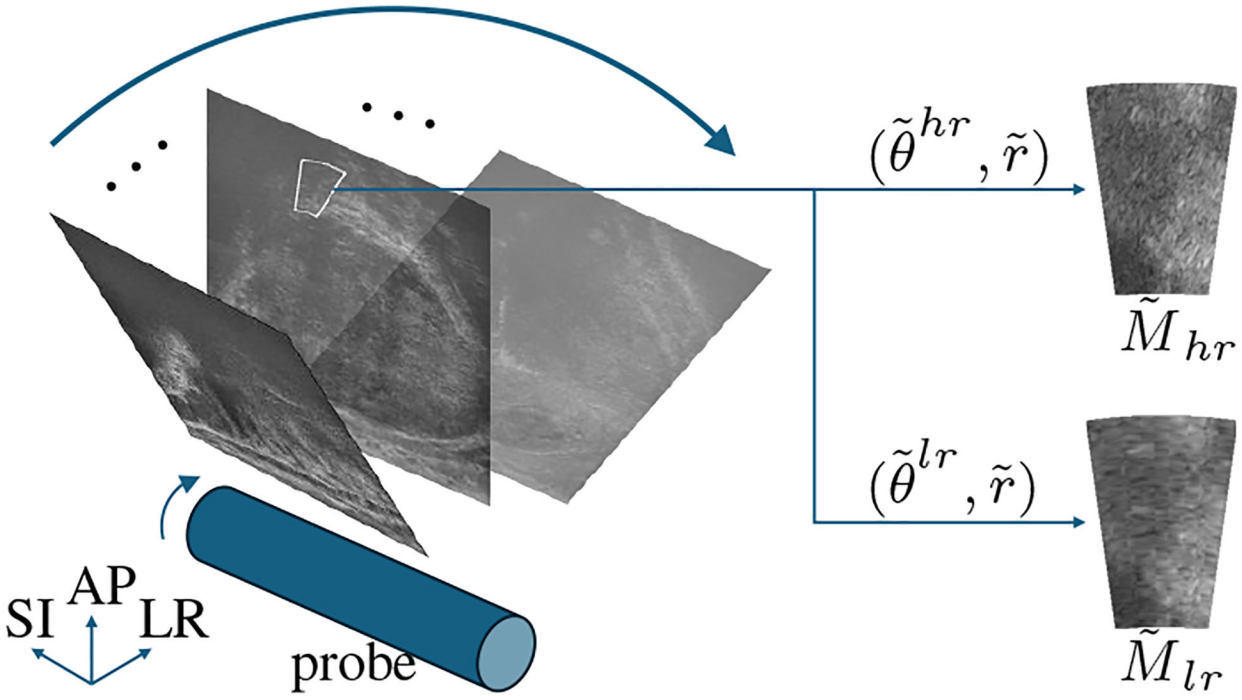

Fig. 4:
Extract LR and HR training patches from acquired slices.

Author Manuscript Author Manuscript Author Manuscript Author Manuscript

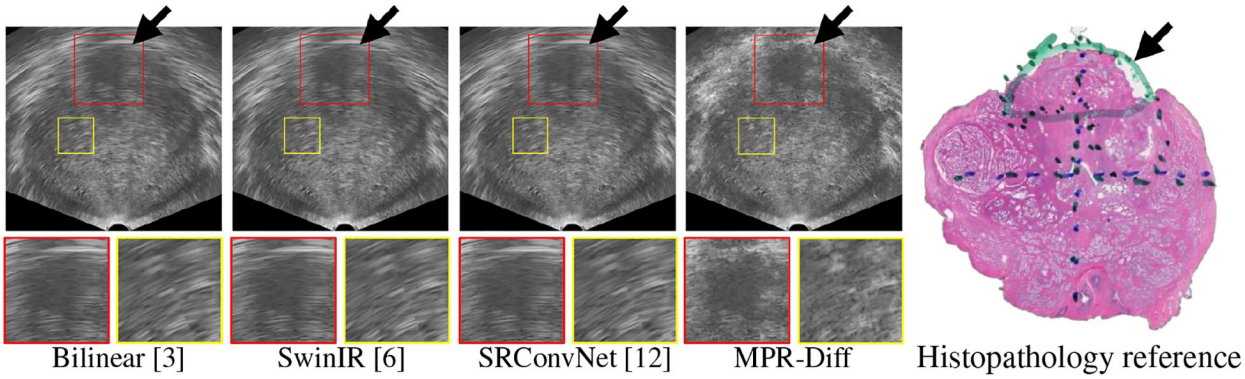

Fig. 5:

Qualitative comparison of different MPR methods. The lesion is annotated by the green circle in the histopathology reference and highlighted within the red box in MicroUS images, indicated by the arrows.

Author Manuscript Author Manuscript Author Manuscript Author Manuscript

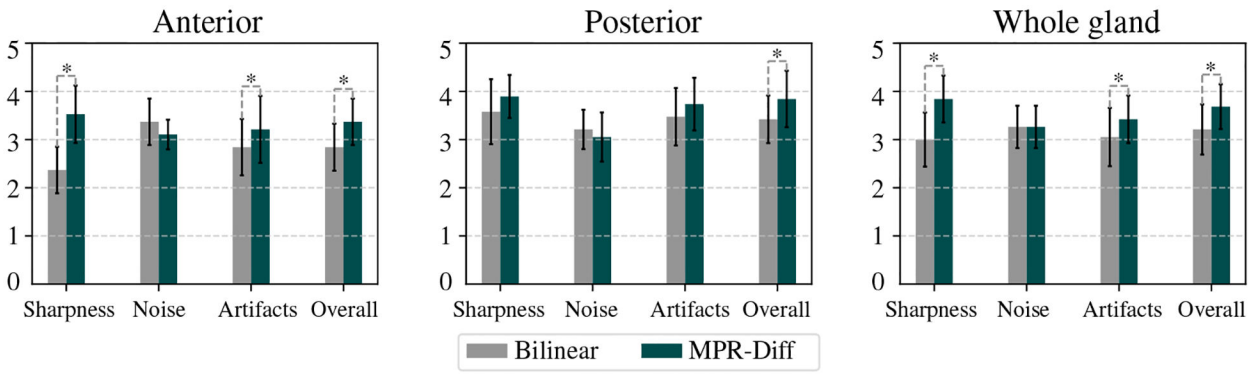

Fig. 6:

Results of the expert reader study. Error bars represent the standard deviations. Comparisons marked with * indicate a statistically significant difference, with $p < 0.05$ calculated using the paired t-test.

Author Manuscript Author Manuscript Author Manuscript Author Manuscript

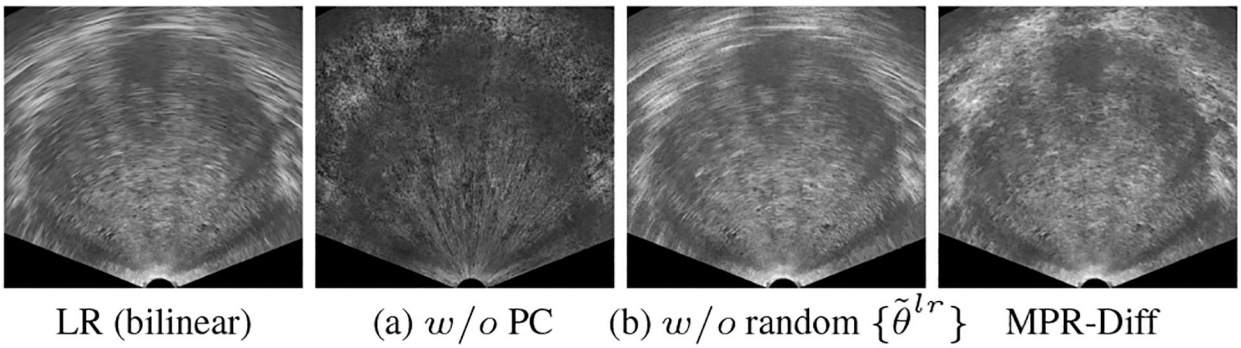

Fig. 7:
Qualitative comparisons in the ablation study.

Author Manuscript

Author Manuscript

Author Manuscript

Author Manuscript

Table 1:

Quantitative comparison between MPR-Diff and other methods.

Method	Sharpness [14] ($\times 10^2$) ↑	PIQUE [15] ↓
Bilinear [3]	4.35	26.44
SwinIR [6]	4.36	26.24
SRConvNet [12]	4.39	25.18
MPR-Diff	**4.44**	**19.47**